Direct observation of the discrete energy spectrum of two lanthanide-based single-chain magnets by far-infrared spectroscopy

Sabrina Haas, Eric Heintze, Sina Zapf, Boris Gorshunov,* Martin Dressel, and Lapo Bogani
1. Physikalisches Institut, Universität Stuttgart, Pfaffenwaldring 57, D-70550 Stuttgart, Germany
(Received 13 February 2014; revised manuscript received 24 April 2014; published 7 May 2014)

The far-infrared optical transmission has been studied for two lanthanide-based single-chain magnets DyPhOPh and TbPhOPh in the frequency range between 3 and 80 cm^{-1}. The spectra were acquired at temperatures between 2 and 80 K and magnetic fields up to 6 T. Based on their magnetic field dependence in DyPhOPh two of the observed absorption lines are identified as transitions inside the crystal field split Dy^{3+} ground multiplet $^6H_{15/2}$, coupled to the neighboring spins. In TbPhOPh one transition was observed inside the crystal-field-split Tb^{3+} ground multiplet $^7F_6$. The results allow a spectroscopic investigation of the role of single-ion anisotropy and exchange in Glauber dynamics.

DOI: 10.1103/PhysRevB.89.174409 PACS number(s): 75.10.Pq, 75.40.Cx, 75.40.Gb, 75.50.Xx

I. INTRODUCTION

Since the first observation of slow relaxation in a single-ion lanthanide compound [1], the family of lanthanides has moved into the focus of research in molecular magnetism [2–11]. Their unquenched orbital momenta can cause strong magnetic anisotropy [12], a necessary requirement for slow relaxation in molecular magnetic materials [13–15]. Although trivalent lanthanide centers show weak coupling to other spins, a wide range of single-molecule magnets [16–19] and single-chain magnets [20,21] have been synthesized from them; such systems constitute a thriving field of research, with many still-open questions regarding both their chemistry and magnetism.

A key issue for the investigation of the relaxation process in molecular materials is the determination of the energy spacings and the nature of the spin levels. In single-ion lanthanide magnets the relaxation process is proposed to take place by thermally assisted mechanisms, via an excited real state (e.g., Orbach process) with additional contributions due to quantum tunneling of the magnetization [22,23]. For the thermal relaxation process, the effective energy barrier observed in magnetization measurements has an upper limit in the energy of the spin excited state; it is usually lower due to the contribution of underbarrier processes.

For single-chain magnets with anisotropic building blocks the pure Ising treatment of Glauber has been extended to include an intrinsic anisotropy barrier of the constituents and the possible presence of transverse components [24]. A major improvement was achieved by further including the finite length of the single-chain magnet. In this way a finite-size regime can be identified [25], where the correlation length ξ exceeds the chain length L ($\xi \gg L$), and an infinite-size dynamic regime, where ξ is much smaller than L ($\xi \gg L$). The relaxation time varies when going from the infinite-size regime, corresponding to the Glauber model with nucleation of the magnetic excitation inside the chain, to the finite-size regime, with nucleation at the chain ends [21,24–27]. Once nucleation started with a certain energy barrier, the relaxation process takes place via a random walk of the domain walls, at no energy cost. The role of the single-ion anisotropy in the random walk process, however, remains an open problem. A rigorous theoretical treatment of the situation is still lacking, and only heuristic arguments [27] have been used to explain the experimental data, up to now.

At present there is little understanding of how single-ion and collective dynamic processes are intertwined in single-chain magnets, in part because modeling is hampered by the presence of very high spin-orbit coupling [28]. In most rare-earth-based molecular magnets with a low-symmetry environment, like the compounds studied here, these difficulties are now being overcome by new models that are slowly reaching the necessary precision and reliability. In particular, electrostatic models [5,23,29] and complete active space self-consistent field calculations seem promising for the determination of the energy level spacing, but are still in development and need the necessary experimental validation.

On the other hand, standard experiments usually do not yield a clear picture of the energy level spacing. Far-infrared spectroscopy now offers a unique possibility to directly obtain the energy-level splittings between the low-lying crystal field split states without any further assumptions of the symmetry or the coupling to the neighboring spins. If the energy of an incoming photon corresponds to the energy difference between two states, the photon is absorbed. The technique has already been used to determine the crystal field of rare-earth iron garnets [30,31] and rare-earth double nitrates [32]. In the field of molecular magnetism a comparable technique, dubbed frequency-domain magnetic resonance, was established for transition-metal single-molecule magnets [33–36]. Nevertheless, the use of these techniques to study single-chain magnets is still unexplored. Here we use far-infrared spectroscopy to explore the low-lying energy levels of two single-chain magnets, containing highly-anisotropic Dy^{3+} and Tb^{3+} ions.

II. EXPERIMENTS AND ANALYSIS

A. LnPhOPh single-chain magnets

In this study we will focus on the Tb and Dy derivatives of the lanthanide-based isostructural single-chain-magnet

*Permanent address: A. M. Prokhorov Institute of General Physics, Russian Academy of Sciences, Moscow 119991, and Moscow Institute of Physics and Technology (State University), Dolgoprudny, Moscow Region 141700, Russia.

 ©2014 American Physical Society

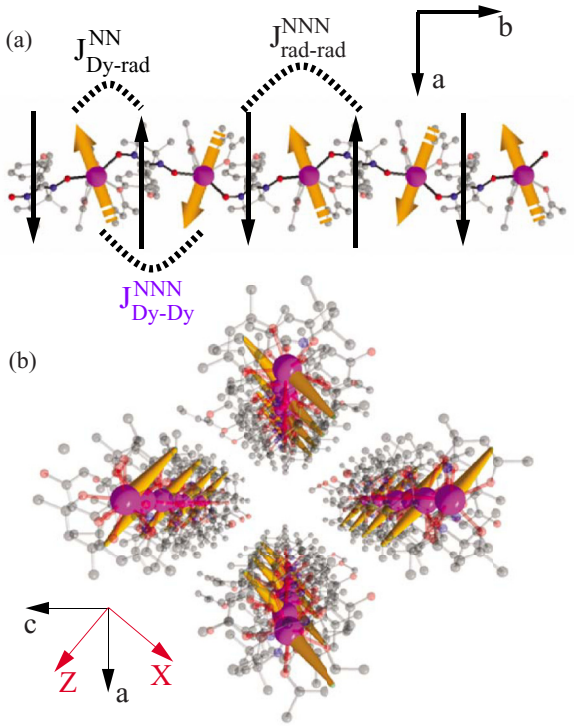

FIG. 1. (Color online) (a) Sketch of the spin alignment in DyPhOPh in the *ab* plane, with bold orange arrows indicating the Dy^{3+} spins and thin black arrows the radical spins. The magnetic interactions are labeled as used in the text. (b) View of the crystal structure of DyPhOPh, with the fluorine and hydrogen atoms omitted for clarity. The Dy ions are colored magenta, N blue, O red, and C gray (after Ref. [39]).

family $[Ln(hfac)_3\{NIT(C_6H_4OPh)\}]$ where hfac is hexafluoroacetylacetonate and $NIT(C_6H_4OPh)$ stands for the nitronyl-nitroxide radical 2-*R*-4,4,5,5-tetramethyl-4,5-dihydro-1H-imidazolyl-1-oxil-3-oxide containing $R = C_6H_4OPh$. The structure of these compounds consists of alternating Dy^{3+} ions bridged by purely organic nitronyl-nitroxide radicals, as sketched in Fig. 1. Along the alternating units, the Dy^{3+} ions and the radicals are coupled ferromagnetically by J^{NN}_{Dy-rad}, while the next-nearest-neighbor couplings between the Dy^{3+} centers, J^{NNN}_{Dy-Dy}, and the radicals, $J^{NNN}_{rad-rad}$, are antiferromagnetic.

The lanthanide-based single-chain magnet DyPhOPh has previously been characterized in detail by static and dynamic magnetic susceptibility measurements [37–39]. Based on angle-dependent investigations the static magnetic behavior of DyPhOPh was modeled by a classical Hamiltonian for the coupling between the spins [38]. The anisotropy of the system is largely given by the Dy^{3+} ions, as revealed from modeling the angular dependence of the magnetic behavior at low temperature, by neglecting the radical contribution to the magnetization and taking into account only the Dy^{3+} spins. The radical contribution to the magnetization is expected to be negligible because of the strong antiferromagnetic coupling between them. Dy^{3+} ions behave as Ising spin centers, with the local easy axis tilted by 75° off the crystallographic *b* axis, which runs parallel to the chain axis. This leads to weak ferromagnetism along the *b* axis, as also observed in other single-chain magnets [40]. Above 10 K the Dy^{3+} spins behave as paramagnetic spin centers, with a local easy axis. Around 10 K the coupling between the Dy^{3+} spins starts to play a significant role, leading to an uncompensated moment along the *b* axis. The next-nearest-neighbor coupling constant was determined as $J^{NNN}_{Dy-Dy} = 17\,cm^{-1}$ with the Dy^{3+} spins taken as $S_{eff} = 1/2$ within a Heisenberg spin Hamiltonian with high anisotropy, as discussed previously in the literature [39].

On lowering the temperature the spin-spin correlation grows exponentially, until it reaches the limit imposed by the presence of defective sites in the chains. These are due to crystalline displacements and the possibility of oxidizing/reducing the radical parts. Both effects are introduced into the modeling of the system as a random dilution of the chain, which produces a geometrical distribution of chain lengths. The occurrence probability of the defects has been assessed very carefully on similar systems by diamagnetic doping [25,26]. For rare-earth-based SCMs a geometrical limitation was extracted by noticing that the geometric length provides a limit for the growth of the spin correlation length. Scaling procedures thus provided an average chain length of about 3000 unit cells in Dy and Tb PhOPh [37,38].

The TbPhOPh chain exhibits a similar behavior, but has not received such high levels of attention. It is almost perfectly isostructural with the Dy compound, and also behaves as a collection of highly anisotropic spin centers with an Ising character. In contrast to Dy^{3+}, the Tb^{3+} analog is a non-Kramers ion with the ground multiplet $^7F_6$ with $J = 6$. In principal, low-symmetry crystal fields can lift the degeneracy completely, leading to $(2J + 1) = 13$ crystal-field levels. However, at low temperatures the Tb^{3+} ion is often modeled as a $S = 1$ spin [38] with a non-Kramers ground-state doublet. TbPhOPh does not show a crossover in the dynamic properties, although it provides a large opening of the hysteresis loop at 1.5 K. Here it is used as a comparison to the Dy analog, and to apply the knowledge obtained from DyPhOPh to a system which has received less attention, both theoretically and experimentally.

B. THz and infrared transmission spectroscopy

The optical transmission spectra were acquired with a Bruker IFS 113v Fourier Transform spectrometer connected to an Oxford Spectromag 4000 Split-Coil Magnet with mylar windows. In the frequency range 20–80 cm^{-1} we used unpolarized light detected by an He cooled bolometer with a resolution of 0.5 cm^{-1}. Magnetic fields were applied up to 6 T in Voigt geometry, i.e., the propagation direction is perpendicular to the external field. Each spectrum was normalized by a reference spectrum taken through an empty aperture of equal size. The specimen itself is pellet pressed out of microcrystalline powder. In Fig. 2 the transmissions spectra are displayed at different temperatures and magnetic fields. At lower frequencies, we have employed a coherent source THz spectrometer as described previously [34,36,41]. The transmission spectra acquired at different temperatures are plotted in Fig. 3.

The transmission spectra were fitted using the Fresnel formulas for a plane parallel layer [42]. For the observed

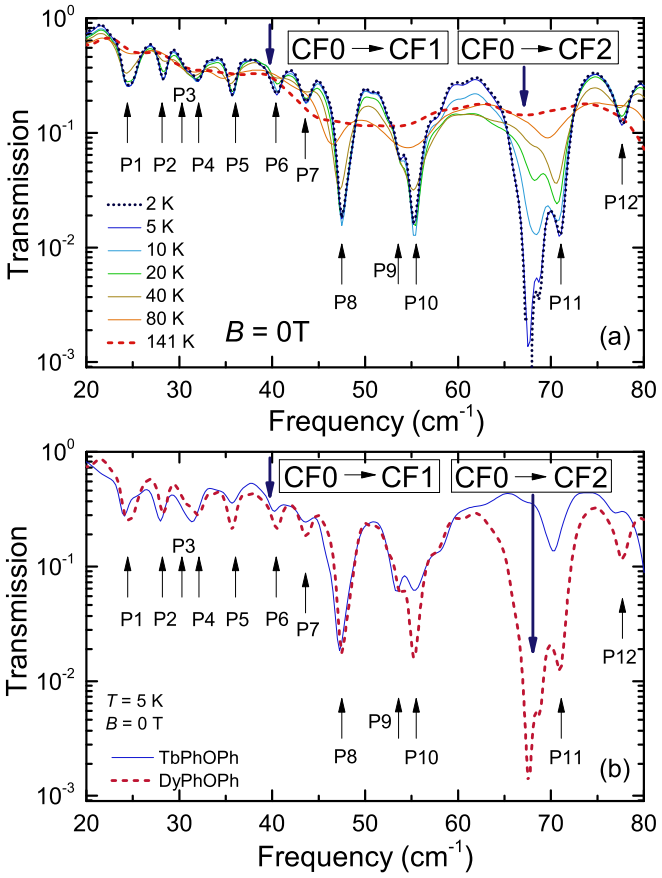

FIG. 2. (Color online) (a) Transmission spectra of a powder pellet of DyPhOPh (thickness 0.54 mm) measured at temperatures between 2 and 141 K without magnetic field. The phonon lines are labeled with P1 through P12 and the electronic absorption lines with CF0→CF1 and CF0→CF2 for the corresponding transitions inside the $^6H_{15/2}$ multiplet. (b) Comparison between the transmission spectra of DyPhOPh (thickness 0.54 mm) and TbPhOPh (thickness 0.40 mm) at $T = 5$ K and $B = 0$ T.

absorption lines, magnetic and electric oscillators where introduced:

$$\epsilon^*(\nu) = \epsilon_1(\nu) + i\epsilon_2(\nu) = \epsilon_\infty + \sum_j \frac{\Delta\epsilon_{i,j}\nu_{i,j}^2}{\nu_{i,j}^2 - \nu^2 + i\nu\gamma_{i,j}}, \quad (1)$$

$$\mu^*(\nu) = \mu_1(\nu) + i\mu_2(\nu) = 1 + \sum_j \frac{\Delta\mu_{i,j}\nu_{i,j}^2}{\nu_{i,j}^2 - \nu^2 + i\nu\gamma_{i,j}}, \quad (2)$$

with the complex dielectric permittivity $\epsilon^*(\nu)$, complex magnetic permeability $\mu^*(\nu)$, the resonance frequency $\nu_{i,j}^2$, and the damping factor $\gamma_{i,j}$. This leads to the refractive index $n^*(\nu) = n_1(\nu) + in_2(\nu) = \sqrt{\epsilon^*\mu^*}$ and the transmission spectrum.

The absorption lines caused by electronic excitations can be distinguished from lattice vibrations by applying a magnetic field that influences only the former one due to the Zeeman effect. The vibronic and phononic absorption lines are then modeled as dielectric oscillators. The electronic transitions inside the $^6H_{15/2}$ multiplet are described by the magnetic oscillator model, in which the contribution to the static

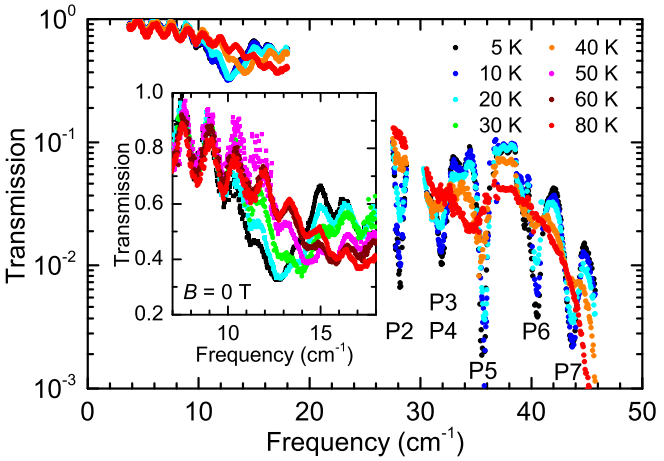

FIG. 3. (Color online) Zero-field transmission spectra of a DyPhOPh pellet (thickness 1.975 mm) acquired at different temperatures in the THz range. Some of the phonon lines are labeled in accord with Fig. 2. The inset shows a magnification of the low-frequency spectral range on a linear scale in order to demonstrate the shift of the 13 cm^{-1} mode as the temperature is reduced to 5 K.

magnetic permeability is given by $\Delta\mu_{i,j}$ [35,43,44]:

$$\Delta\mu_{if} = \frac{8\pi}{3} N_0 \frac{\sum_{\alpha=x,y,z} |\langle f|g_\alpha \mu_B \hat{S}_\alpha|i\rangle|^2}{\hbar\omega_{i,f}} \times \frac{1}{Z}\left[\exp\left\{-\frac{E_f}{k_B T}\right\} - \exp\left\{-\frac{E_i}{k_B T}\right\}\right], \quad (3)$$

with the matrix element of the magnetic moment between the two participating states averaged over the three polarizations of light $\frac{1}{3}\sum_{\alpha=x,y,z}|\langle f|g_\alpha\mu_B\hat{S}_\alpha|i\rangle|^2$, the population difference between the two states $\Delta P = \frac{1}{Z}[\exp\{-\frac{E_f}{k_BT}\} - \exp\{-\frac{E_i}{k_BT}\}]$, and the density N_0 of Ln^{3+} spins.

In single crystals the Zeeman effect leads to a shift of the absorption line, linear with the magnetic field strength. The manifestation of the Zeeman splitting in a powder sample—like the one used in this study—is more complex, because the direction of the magnetic field vector is pointing in a different direction for each crystallite. This leads to a broadening of the lines; the effect is particularly pronounced for low-symmetry centers with high spin-orbit coupling, because the spectroscopic g factor is different for all directions.

The electronic transitions can also contain an electric dipole contribution. These transitions are normally forbidden inside the multiplet by the parity selection rule. However, in the case of low symmetry, the Dy^{3+} ion can be shifted from the center of symmetry, leading to a mixing with excited $4f^{n-1}5d^1$ states into the $4f$ configuration. As both are of opposite parity, this allows electric dipole transitions, as pointed out in the literature [45,46].

III. RESULTS

In order to identify the electronic absorption lines, we first exclude the absorptions caused by phonons. Figure 2(b) displays a comparison between the transmission spectra of the two compounds DyPhOPh and TbPhOPh. Both spectra

reveal absorption lines at essentially the same frequencies (labeled P1 to P12) with only slightly different intensities, giving evidence that both compounds are isostructural with one lanthanide ion replaced by another. The substitution of Dy^{3+} by Tb^{3+} influences the far-infrared phonon spectrum only slightly, because both ions have very similar masses and, in addition, the mass change is compensated by a change in the ionic radius [32]. Further evidence for their phononic or vibronic character can be found in Fig. 2(a): With rising temperature, their resonance frequency slightly decreases due to the thermal expansion of the lattice. The decrease is only around 1 cm^{-1} for most of the lines, as expected for this temperature range [32] (cf. Fig. 2 of the Supplemental Material [49]). In addition, the damping factor increases with temperature, leading to a broadening of the lines.

DyPhOPh. The ground state of Dy^{3+} ions is $^6H_{15/2}$, with half-integer angular momentum. The presence of a low-symmetry crystal field raises the degeneracy of the J multiplet, resulting in $(J + 1/2) = 8$ Kramers doublets [47]. We will restrict our analysis to temperatures below 10 K, when only the lowest-lying doublet is populated. Thus, transitions present in the far-infrared spectrum mainly originate from the lowest Kramers doublet. Furthermore, intrachain spin correlations become more and more important on lowering the temperature, until they reach the geometrical limitations imposed by the finite size of the chains, so that the sample can be considered as formed by segments, on average a few thousands of unit cells long, with antiferromagnetically aligned Dy^{3+} spins, as sketched in Fig. 1. This influences the energy of the crystal-field-split states and thus also the far-infrared response, which probes the collective energy-level structure.

The magnetic field dependence of the transmission spectra at low temperatures is plotted in Fig. 4(a). Normalization of the spectra with respect to the one acquired in zero field [Fig. 4(b)] allows us to identify intensity changes at around 40, 47, 55, and 68 cm^{-1} with an uncertainty of up to 2 cm^{-1}. The features at 40 and 68 cm^{-1} do not coincide with any phonon resonance frequency and are well above the noise level; they can be unambiguously assigned to electronic transitions that are subject to Zeeman splitting in an applied magnetic field. At low temperatures the 68-cm^{-1} absorption splits into two lines at 67.5 and 68.5 cm^{-1} that cannot be simply explained by crystal-field splitting. This fact converses the Kramers degeneracy of the two doublets and gives evidence for an anisotropic exchange coupling acting on the Dy^{3+} spins, that can raise the Kramers degeneracy [48].

We have performed a fit of the zero-field spectrum at $T = 5$ K as discussed above in Sec. II B and the Supplemental Material [49]. For the 40-cm^{-1} line the fit yields a contribution to the static magnetic permeability $\Delta\mu_{01} = 0.0005 \pm 0.0004$ and an averaged matrix element of the magnetic moment of $\frac{1}{3}\sum_{\alpha=x,y,z} |\langle f|g_\alpha \mu_B \hat{S}_\alpha|i\rangle|^2 = (3 \pm 2)\mu_B^2$. The contributions of the 68-cm^{-1} line to the static magnetic permeability is much stronger; we determine for the two parts of the split absorption line $\Delta\mu'_{02} = 0.004 \pm 0.001$ and $\Delta\mu''_{02} = 0.0008 \pm 0.0005$ resulting in an averaged matrix element of the magnetic moment of $\frac{1}{3}\sum_{\alpha=x,y,z} |\langle f|g_\alpha \mu_B \hat{S}_\alpha|i\rangle|^2 = (47 \pm 14)\mu_B^2$.

Unfortunately the magnetic-field-induced changes at 47 and 55 cm^{-1} coincide with the strong phonon resonances P8 and P10, which complicates the analysis significantly. The signatures could be artifacts because the external magnetic field may (to a minor degree) influence phonons, too. In order to resolve this issue, additional information can be obtained when comparing the zero-field data of Tb and Dy: While the spectra coincide for the P8 phonon, they clearly deviate around the P10 mode. This makes it very unlikely that the absorption

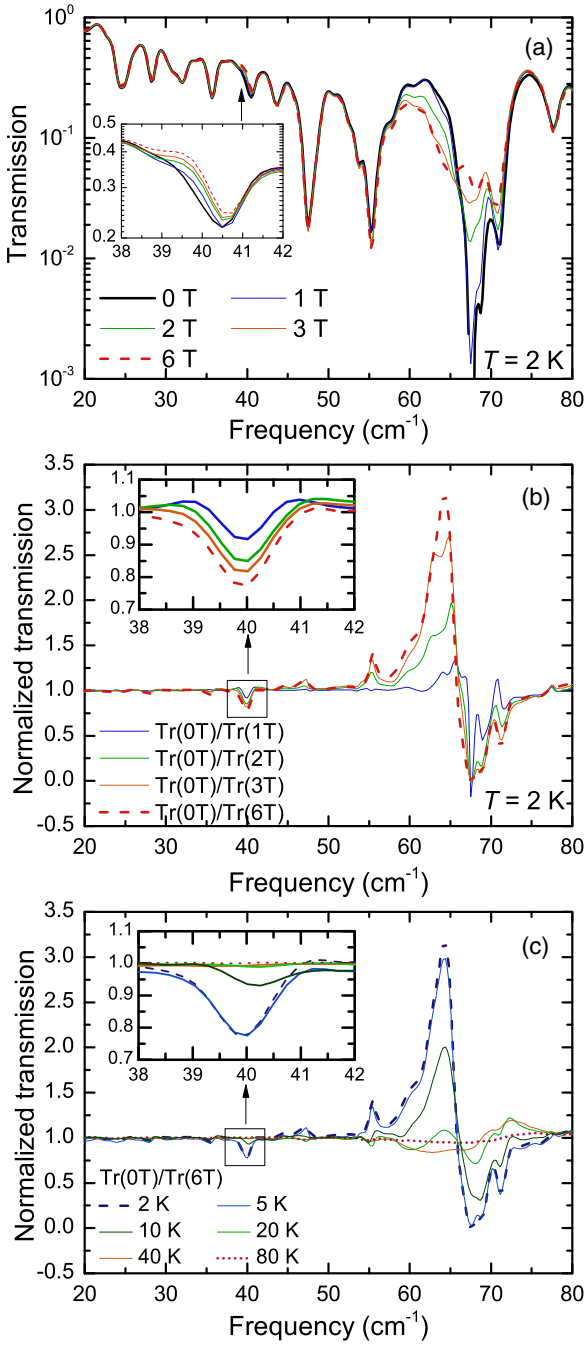

FIG. 4. (Color online) (a) Transmission spectra of DyPhOPh (thickness 0.54 mm) at $T = 2$ K taken at different strength of the magnetic field. (b) Ratios of the transmission spectra of DyPhOPh at $B = 0$ T normalized to spectra with an applied field ($B = 1$ to 6 T) at 2 K. (c) Ratios of the transmission spectra for DyPhOPh of the spectra at $B = 0$ T normalized to spectra with an applied field of $B = 6$ T at temperatures from 2 to 80 K.

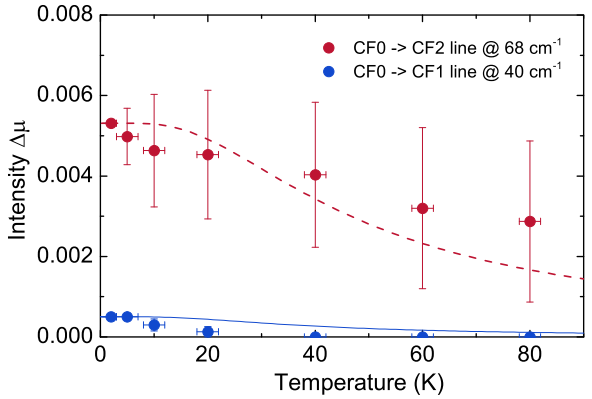

FIG. 5. (Color online) Temperature dependence of the peak intensity for the 68- and 40-cm^{-1} lines of DyPhOPh. The solid lines represent the Boltzmann theory for excitations between two levels of corresponding energy differences. The rather large error bars result from its temperature-dependent line splitting.

feature P8 contains an additional electronic vibration, whereas this scenario is more probable for the P10 mode. Thus we are confident that the 55-cm^{-1} feature results from electronic contributions which are just accidentally located at the same energy as a phonon.

For all electronic absorptions, as the temperature increases, the magnetic field dependence quickly vanishes. This behavior results from the temperature-dependent population of the states that follows a Boltzmann distribution, as demonstrated in Fig. 5 for the clearly identified lines at 40 and 68 cm^{-1}.

We have furthermore extended our measurements to lower energies, covering the THz frequency range, because susceptibility measurements suggested intrachain interaction energies around 10 cm^{-1} also leading to energy level splitting. As demonstrated in Fig. 3, the transmission in the THz frequency range matches the infrared spectra very well. Below 20 cm^{-1}, fringes due to multireflection within the pressed pellet become pronounced. Nevertheless, we clearly observe around 13 cm^{-1} a strong absorption line. Due to its characteristic temperature dependence, this line can be identified as an electronic absorption: As temperature increases, the mode shifts to higher energies in contrast to phonon modes.

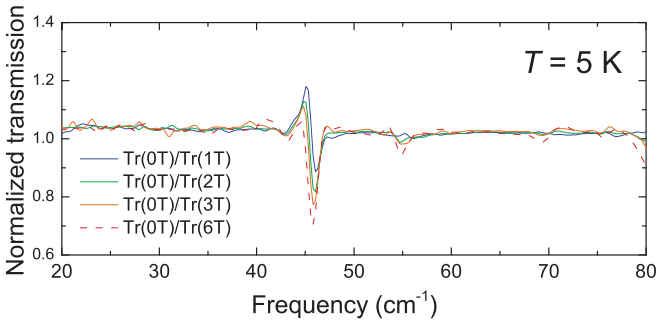

FIG. 6. (Color online) Ratios of the transmission spectra of TbPhOPh (thickness 0.40 mm) at $B = 0$ T normalized to spectra with an applied magnetic field $B = 1$ to 6 T at the lowest temperature $T = 5$ K.

TbPhOPh. The normalized magnetic-field dependence of the transmission spectra at $T = 5$ K are displayed in Fig. 6. One strong electronic absorption line can be clearly identified at $(45 \pm 2)\,\mathrm{cm}^{-1}$. It is situated at the low-frequency shoulder of the phonon P8, and eventually exhibits a splitting into lines at $(43 \pm 2)\,\mathrm{cm}^{-1}$ and $(46 \pm 2)\,\mathrm{cm}^{-1}$. The other features visible at $(55 \pm 2)\,\mathrm{cm}^{-1}$ and $(70 \pm 2)\,\mathrm{cm}^{-1}$ are much weaker and coincide again with strong phonon absorption lines.

IV. DISCUSSION

We interpret our observations in the framework of previous experimental results on the static and dynamic behavior of DyPhOPh and TbPhOPh and theoretical calculations. The energy scale of the intrachain interactions has already been estimated [37–39] by angular-dependent magnetization measurements and scaling laws of the molecular susceptibility. The resulting intrachain interaction energies are $(13 \pm 2)\,\mathrm{cm}^{-1}$ for the DyPhOPh chain and $(7 \pm 2)\,\mathrm{cm}^{-1}$ for the case of TbPhOPh.

Complete active space self-consistent field (CASSCF) calculations for the DyPhOPh chain yield several doublets above the ground state, with the first two placed within our energy range, at 40 cm^{-1} and 59 cm^{-1} [39]. The actual content of the levels and the possible presence of a mixture of spin states has not been determined, and remains an open issue. However, the corresponding states in lanthanide compounds will not be pure eigenfunctions of S_z (or J_z), due to the presence of spin-orbit coupling and the low-symmetry ligand field around the rare earth. Thus radiation-induced spin-flip processes and transitions from the ground to the second-excited doublet get allowed [31,32]. CASSCF calculations on the TbPhOPh chain are still missing.

DyPhOPh. On this basis we can assign the electronic absorption lines determined by our spectroscopic experiments at 13, 40, and 68 cm^{-1} as well as possibly at 55 cm^{-1} and suggest the energy diagram sketched in Fig. 7. The lowest-energy line at 13 cm^{-1} corresponds to a radiation-induced

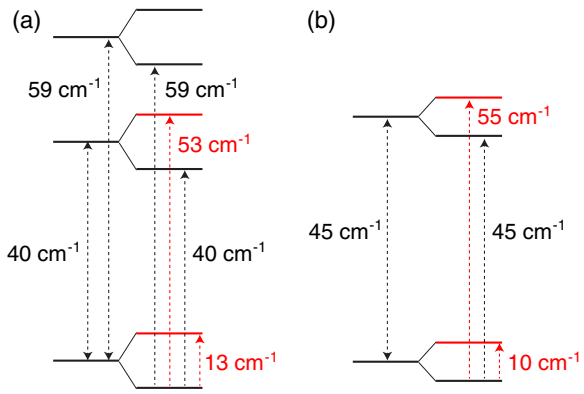

FIG. 7. (Color online) (a) Energy level spacing for DyPhOPh, as calculated with CASSCF methods and considering the presence of intrachain interactions. The transitions and levels that imply a spin flip, are marked in red. (b) Level spacing of TbPhOPh, as extracted from the far-infrared measurements.

spin-flip process, which perfectly agrees with the previous report on the intrachain interaction energy [39]. As discussed above, this process is allowed for mixed states. The two absorption lines at 40 and 68 cm^{-1} correspond to an excitation from the ground to the first and second excited Kramers doublet, respectively. Those values compare well with the CASSCF calculations. Finally, the possible absorption line at 55 cm^{-1} perfectly fits to a transition from the ground state to the first excited doublet, including a spin flip. The observed spin flip at 13 cm^{-1} already confirmed the impurity of the states and strengthens this interpretation.

TbPhOPh. The picture that emerges from our spectroscopic data on DyPhOPh can now be applied to also interpret the TbPhOPh spectra, where no CASSCF calculations of the level spacing have been published yet. The features at 45 cm^{-1} and 55 cm^{-1} can be assigned to the transition to an excited doublet and to the corresponding spin-flip transition. The spacing between the lines matches the 7 cm^{-1} energy extracted from the static susceptibility data.

Energy scales of dynamic properties. Although the present data provide information primarily on the statics of the chains, it is instructive to compare these results to the dynamic properties and the related energy scales. In the Glauber model extended to single-ion anisotropy, it has been proposed [21,27] that the relaxation time is $\tau = \tau_0 \cdot \exp\{(4|J|S^2 + \Delta)/k_B T\}$ in the infinite size regime and $\tau = \tau_0^* \cdot \exp\{(2|J|S^2 + \Delta)/k_B T\}$ in the finite size regime, where Δ stands for a single ion contribution. For DyPhOPh, ac susceptibility measurements reveal two distinguishable temperature regimes: at lowest temperatures, an Arrhenius behavior is found with a relaxation barrier of $\Delta' = (30 \pm 1)\,cm^{-1}$. Above $T = 3.7$ K, a crossover with a relaxation barrier of $\Delta'' = (48 \pm 1)\,cm^{-1}$ is observed [37], which is ascribed to a transition from the finite to the infinite size regime, with the presence of single-ion anisotropy contributions. For TbPhOPh, the relaxation barrier determined via ac susceptibility [38] is $\Delta = (32 \pm 1)\,cm^{-1}$.

It is important to recall that in order to create a conventionally dipole-forbidden excitation, one needs to overcome the single-ion anisotropy energy. The spectroscopic investigation of DyPhOPh reveals the first state connected to such processes at approximately 55 cm^{-1}, slightly above the ~48 cm^{-1} value extracted from the dynamics. For TbPhOPh, the relaxation barrier determined via ac susceptibility is $\Delta = 32\,cm^{-1}$ [38], which again lies below the observed transition. In both cases, phonon lines appear at close energies, which is predicted to support the spin-flip processes [50].

We want to point out that in the literature, there is a discrepancy between the barriers for the finite-size and infinite regimes observed experimentally [37,38] and the values expected from the heuristic arguments on the activated dynamics in the presence of single-ion anisotropy [27]. This is largely to be attributed to the still noncomplete treatment of single-ion anisotropy in Glauber dynamics, which still relies on intuitive arguments and could possibly lead to discrepancies whenever the single-ion energy spacings are large compared to the exchange interaction, as in the present case.

V. CONCLUSION

We have shown that far-infrared transmission spectroscopy can be used as an efficient tool to study the energy levels of low-symmetry lanthanide ions. The information on the level spacing, and the temperature and field dependence of the absorption lines is compared to *ab initio* calculations and previous dc and ac susceptibility measurements. The excellent agreement observed provides a direct, spectroscopic validation of these theoretical techniques and corroborates the predictions made up to now. In addition to the transitions associated with the crystal-field splitting of the Dy^{3+} ground multiplet $^6H_{15/2}$, weaker transitions associated with the coupling to neighboring spins and spin-flip processes can be identified in our spectra. The observed energies agree well with the values obtained from the magnetization dynamics, providing a validation of the proposed activation processes. At the same time, discrepancies are observed with the predictions made by presently available heuristic models [27] of Glauber dynamics in the presence of strong single-ion anisotropy. This should prompt a more thorough and rigorous examination of these situations. On the experimental level, this work provides, with the spectroscopic accuracy, the energy levels of the system, and allows one to directly determine the energy scales involved without any particular model assumption. This can then be used to validate a complete, nonheuristic model of Glauber dynamics coupled to single-ion anisotropy. In addition, the simultaneous observation of phononic lines in the proximity of the barrier and their influence on the dynamic process can now be investigated theoretically. Extension of the techniques here demonstrated to other systems will possibly lead to a full microscopic picture of the relaxation mechanism, which is presently still lacking for Glauber's model.

The magnetic modes observed provide the possibility of addressing the problems of single-ion anisotropy in single-chain magnets, where mixed solitons and spin-wave modes can lead to magnetic excitations [24]. Single-crystal measurements using torque-detected EPR [51] are underway to study such effects. Eventually, the technique demonstrated here also offers a possibility for the spectroscopic investigation of the magneto-optical effects recently observed in single-chain magnets [52] and other molecular magnetic materials [53,54]. Extension of the present methods to pulsed techniques might lead to optical control coupled to a far-IR readout of chain states, which would be essential for the implementation of the proposed quantum computing schemes on chains [55,56].

ACKNOWLEDGMENTS

We thank J. van Slageren for helpful discussions. We acknowledge financial support from the Alexander von Humboldt-Foundation (Sofja Kovalevskaja Prize), the Deutsche Forschungsgemeinschaft (DR228/43-1 via SPP-1601), the Baden-Württemberg Stiftung (Kompetenznetz Funkionelle Nanostrukturen), and the European Research Council (ERC-StG 338258 "OptoQMol").

[1] N. Ishikawa, M. Sugita, T. Ishikawa, S. Koshihara, and Y. Kaizu, J. Am. Chem. Soc. **125**, 8694 (2003).

[2] A. Mishra, W. Wernsdorfer, K. A. Abboud, and G. Christou, J. Am. Chem. Soc. **126**, 15648 (2004).

[3] C. M. Zaleski, E. C. Depperman, J. W. Kampf, M. L. Kirk, and V. L. Pecoraro, Angew. Chem. Int. Ed. **43**, 3912 (2004).

[4] M. A. AlDamen, J. M. Clemente-Juan, E. Coronado, C. Martí-Gastaldo, and A. Gaita-Ariño, J. Am. Chem. Soc. **130**, 8874 (2008).

[5] M. A. AlDamen, S. Cardona-Serra, J. M. Clemente-Juan, E. Coronado, A. Gaita-Ariño, C. Martí-Gastaldo, F. Luis, and O. Montero, Inorg. Chem. **48**, 3467 (2009).

[6] P.-H. Lin, T. Burchell, L. Ungur, L. Chibotaru, W. Wernsdorfer, and M. Murugesu, Angew. Chem. Int. Ed. **48**, 9489 (2009).

[7] T. C. Stamatatos, S. J. Teat, W. Wernsdorfer, and G. Christou, Angew. Chem. Int. Ed. **48**, 521 (2009).

[8] J. J. Le Roy, M. Jeletic, S. I. Gorelsky, I. Korobkov, L. Ungur, L. F. Chibotaru, and M. Murugesu, J. Am. Chem. Soc. **135**, 3502 (2013).

[9] S. Cardona-Serra, J. M. Clemente-Juan, E. Coronado, A. Gaita-Ariño, A. Camón, M. Evangelisti, F. Luis, M. J. Martínez-Pérez, and J. Sesé, J. Am. Chem. Soc. **134**, 14982 (2012).

[10] G. Poneti, K. Bernot, L. Bogani, A. Caneschi, R. Sessoli, W. Wernsdorfer, and D. Gatteschi, Chem. Commun. **18**, 1807 (2007).

[11] J. D. Rinehart, M. Fang, W. J. Evans, and J. R. Long, J. Am. Chem. Soc. **133**, 14236 (2011).

[12] L. Sorace, C. Benelli, and D. Gatteschi, Chem. Soc. Rev. **40**, 3092 (2011).

[13] D. Gatteschi and R. Sessoli, Angew. Chem., Int. Ed. **42**, 268 (2003).

[14] D. Gatteschi, R. Sessoli, and J. Villain, *Molecular Nanomagnets* (Oxford University Press, Oxford, 2006).

[15] J. D. Rinehart and J. R. Long, Chem. Sci. **2**, 2078 (2011).

[16] D. N. Woodruff, R. E. P. Winpenny, and R. A. Layfield, Chem. Rev. **113**, 5110 (2013).

[17] R. Sessoli and A. K. Powell, J. Coord. Chem. **253**, 2328 (2009).

[18] F. Habib and M. Murugesu, Chem. Soc. Rev. **42**, 3278 (2013).

[19] N. Ishikawa, Polyhedron **26**, 2147 (2007).

[20] L. Bogani, A. Vindigni, R. Sessoli, and D. Gatteschi, J. Mater. Chem. **18**, 4750 (2008).

[21] C. Coulon, H. Miyasaka, and R. Clérac, in *Single-Molecule Magnets and Related Phenomena* (Structure and Bonding, Vol. 122), edited by R. Winpenny (Springer, Berlin, 2006), p. 163.

[22] N. Ishikawa, M. Sugita, T. Ishikawa, S. Koshihara, and Y. Kaizu, J. Phys. Chem. B **108**, 11265 (2004).

[23] R. J. Blagg, L. Ungur, F. Tuna, J. Speak, P. Comar, D. Collison, W. Wernsdorfer, E. J. L. McInnes, L. F. Chibotaru, and R. E. P. Winpenny, Nat. Chem. **5**, 673 (2013).

[24] A. Vindigni, Inorg. Chim. Acta **361**, 3731 (2008).

[25] L. Bogani, A. Caneschi, M. Fedi, D. Gatteschi, M. Massi, M. A. Novak, M. G. Pini, A. Rettori, R. Sessoli, and A. Vindigni, Phys. Rev. Lett. **92**, 207204 (2004).

[26] L. Bogani, R. Sessoli, M. G. Pini, A. Rettori, M. A. Novak, P. Rosa, M. Massi, M. E. Fedi, L. Giuntini, A. Caneschi, and D. Gatteschi, Phys. Rev. B **72**, 064406 (2005).

[27] C. Coulon, R. Clérac, L. Lecren, W. Wernsdorfer, and H. Miyasaka, Phys. Rev. B **69**, 132408 (2004).

[28] G. Cucinotta, M. Perfetti, J. Luzon, M. Etienne, P.-E. Carl, A. Caneschi, G. Calvez, K. Bernot, and R. Sessoli, Angew. Chem. Int. Ed. **51**, 1606 (2012).

[29] J. J. Baldovi, J. J. Borras-Almenar, J. M. Clemente-Juan, E. Coronado, and A. Gaita-Ariño, J. R. Soc. Dalton Trans. **41**, 13705 (2012).

[30] A. J. Sievers and M. Tinkham, Phys. Rev. **129**, 1995 (1963).

[31] J. Yamamoto, B. T. Smith, and E. E. Bell, J. Opt. Soc. Am. **64**, 880 (1974).

[32] D. Bloor and J. Campbell, Chem. Phys. **54**, 3268 (1971).

[33] A. Mukhin, B. Gorshunov, M. Dressel, C. Sangregorio, and D. Gatteschi, Phys. Rev. B **63**, 214411 (2001).

[34] J. van Slageren, S. Vongtragool, B. Gorshunov, A. A. Mukhin, N. Karl, J. Krzystek, J. Telser, A. Müller, C. Sangregorio, D. Gatteschi, and M. Dressel, Phys. Chem. Chem. Phys. **5**, 3837 (2003).

[35] N. Kirchner, J. van Slageren, and M. Dressel, Inorg. Chim. Acta **360**, 3813 (2007).

[36] J. Slageren, in *EPR Spectroscopy: Applications in Chemistry and Biology* (Topics in Current Chemistry, Vol. 321), edited by M. Drescher and G. Jeschke (Springer, Berlin, 2012), p. 199.

[37] L. Bogani, C. Sangregorio, R. Sessoli, and D. Gatteschi, Angew. Chem. Int. Ed. **117**, 5967 (2005).

[38] K. Bernot, L. Bogani, A. Caneschi, D. Gatteschi, and R. Sessoli, J. Am. Chem. Soc. **128**, 7947 (2006).

[39] K. Bernot, J. Luzon, A. Caneschi, D. Gatteschi, R. Sessoli, L. Bogani, A. Vindigni, A. Rettori, and M. G. Pini, Phys. Rev. B **79**, 134419 (2009).

[40] K. Bernot, J. Luzon, R. Sessoli, A. Vindigni, J. Thion, S. Richeter, D. Leclercq, J. Larionova, and A. van der Lee, J. Am. Chem. Soc. **130**, 1619 (2008).

[41] B. P. Gorshunov, A. Volkov, I. E. Spektor, A. S. Prokhorov, A. A. Mukhin, M. Dressel, S. Uchida, and A. Loidl, Int. J. Infrared Millimeter Waves **26**, 1217 (2005).

[42] M. Dressel and G. Grüner, *Electrodynamics of Solids* (Cambridge University Press, Cambridge, 2002).

[43] A. A. Mukhin, V. D. Travkin, A. K. Zvezdin, S. P. Lebedev, A. Caneschi, and D. Gatteschi, Europhys. Lett. **44**, 778 (1998).

[44] A. A. Mukhin, A. S. Prokhorov, B. P. Gorshunov, A. K. Zvezdin, V. D. Travkin, and M. Dressel, Phys.-Usp. **45**, 1186 (2002).

[45] B. J. Judd, Phys. Rev. **127**, 750 (1962).

[46] T. D. Kang, E. Standard, K. H. Ahn, A. A. Sirenko, G. L. Carr, S. Park, Y. J. Choi, M. Ramazanoglu, V. Kiryukhin, and S.-W. Cheong, Phys. Rev. B **82**, 014414 (2010).

[47] A. Abragam and B. Bleaney, *Electron Paramagnetic Resonance of Transition Ions* (Oxford University Press, Oxford, 1986).

[48] D. Bloor and G. Copland, Rep. Prog. Phys. **35**, 1173 (1972).

[49] See Supplemental Material at http://link.aps.org/supplemental/10.1103/PhysRevB.89.174409 for more details and examples of the fits.

[50] J. Lehmann and D. Loss, Phys. Rev. B **73**, 045328 (2006).

[51] F. El Hallak, J. van Slageren, and M. Dressel, Rev. Sci. Instr. **81**, 095105 (2010); F. El Hallak, P. Neugebauer, A. L. Barra, J. van Slageren, M. Dressel, and A. Cornia, J. Magn. Res. **223**, 55 (2012).

[52] E. Heintze, F. El Hallak, C. Clauß, A. Rettori, M. G. Pini, F. Totti, M. Dressel, and L. Bogani, Nat. Mater. **12**, 202 (2013).

[53] P. L. Gentili, L. Bussotti, R. Righini, A. Beni, L. Bogani, and A. Dei, Chem. Phys. **314**, 9 (2005).

[54] D. Schweinfurth, F. Weisser, D. Bubrin, L. Bogani, and B. Sarkar, Inorg. Chem. **50**, 6114 (2011).

[55] Y. Tserkovnyak and D. Loss, Phys. Rev. A **84**, 032333 (2011).

[56] C. Cervetti, E. Heintze, and L. Bogani, Dalton Trans. **43**, 4220 (2014).